Electron and hole traps in yttrium orthosilicate single crystals: The critical role of Si-unbound oxygen

V. V. Laguta,[1] M. Buryi,[1] J. Rosa,[1] D. Savchenko,[1] J. Hybler,[1] M. Nikl,[1] S. Zazubovich,[2] T. Kärner,[2]
C. R. Stanek,[3] and K. J. McClellan[3]

[1]*Institute of Physics AS CR, Cukrovarnicka 10, Prague, 16200, Czech Republic*
[2]*Institute of Physics, University of Tartu, Riia 142, 51014 Tartu, Estonia*
[3]*Los Alamos National Laboratory, Los Alamos, New Mexico 87545 USA*

We studied the processes of hole and electron trapping in yttrium orthosilicate Y_2SiO_5 single crystals using continuous wave and pulse electron spin resonance methods. We show that holes created by x-ray irradiation at low temperatures ($T < 80$ K) are preferably self-trapped at Si-unbound oxygen ions in the form of O^- centers. Under irradiation at higher temperatures (200–290 K), the holes are trapped at the Si-unbound oxygen ions in the vicinity of perturbing defects such as yttrium vacancies and impurity ions forming a variety of O^- centers with thermal stability up to room and higher temperatures. We have also found that under x-ray irradiation at $T < 60$ K, electrons are preferably trapped in the vicinity of Si-unbound oxygen ion vacancies and partly trapped also at Mo impurity ions in the form of F^+-type and Mo^{5+} centers, respectively. The trapped electrons are thermally released from the F^+ centers at 75–90 K, thus giving rise to a thermally stimulated luminescence peak at these temperatures. We assume that this process is realized without excitation of the electrons to the conduction band. The spectroscopic parameters (g and hyperfine tensors) of all the investigated centers have been determined as well. Electron spin resonance measurements of electron and hole traps in the related compound lutetium orthosilicate (Lu_2SiO_5) are discussed as well.

I. INTRODUCTION

In last two decades, considerable attention has been given to the study of cerium-doped oxyorthosilicates, Lu_2SiO_5 (LSO) and Y_2SiO_5 (YSO) and their solid solutions [1–7]. A unique combination of high density (7.4 g/cm^3 for LSO), short scintillation decay time (~40 ns), high light output (3.5–4 times that of bismuth germanate [BGO]), and satisfactory energy resolution makes this family of scintillation crystals suitable for the fast detection of high-energy gamma rays [8]. Besides, research activities connected with YSO have been related to rare-earth- (Ce^{3+}, Eu^{3+}, etc.) doped crystals to be used as blue phosphors [9,10] and to Cr^{4+}-doped crystals to be applied as a saturable-absorber Q-switch laser [11]. Recently, Yb^{3+}-doped YSO and LSO silicates were considered as efficient diode-pumped high-power femtosecond lasers [12]. It was reported that they provide up to 2.6 W of average output power with 200–260 fs pulse durations, leading to 17% overall optical efficiency, values that are probably the highest ever obtained for classical fiber-coupled diode-pumping configuration.

Although LSO/YSO crystals have attractive laser and scintillation properties, they show a fairly strong afterglow. This afterglow and corresponding thermally stimulated luminescence (TSL) peaks were tentatively ascribed to the traps containing oxygen vacancies [13,14] as well as to the self-trapped excitons and holes [15]. In particular, it was found that the intrinsic ultraviolet luminescence, attributed to radiative recombinations of electrons with the self-trapped holes (STHs), is quenched at the temperatures exceeding 100 K, indicating a low thermal stability of the STHs. However, the charge trapping mechanism and the origin of the corresponding traps have not been convincingly proved yet in both YSO and LSO lattices due to the lack of information, which could be provided, for example, by electron spin

resonance (ESR) experiments. The ESR data that exist for these important materials are limited to the description of incorporation of Ce^{3+} ions [16,17], measurement of powdered samples [14,18], and study of Er^{3+} impurity and its hyperfine (HF) interaction [19]. In particular, only an ESR signal ascribed to an electron trapped at an oxygen vacancy (F^+ center) was reported in x-ray irradiated LSO and YSO powdered samples [14]. However, no single crystal measurements were performed, which could convincingly prove the origin of the x-ray induced defects.

There were also theoretical calculations of electronic structure of YSO and LSO, which predict possible configurations of charge trapping centers. In particular, the electronic structure and bonding of YSO were studied by DFT calculations [20]. It was found that the bottom of the conduction band is predominantly built from Y atomic orbitals, while the top of the valence band was built from O orbitals. Such electronic structure favors localization of electrons and holes at Y and O ions, respectively. Besides, it was shown that the Y-O bonding is relatively weak.

The oxygen vacancies were modeled by DFT calculations in LSO [21], which show that the Si-unbound oxygen vacancy (V_{O5}) has the lowest formation energy compared to the four oxygen vacancies belonging to the SiO_4 tetrahedron. The presence of the oxygen vacancies can induce extra states in the band gap. The 2+ charge state vacancies are energetically favorable and show lower formation energies with respect to the neutral vacancies [21]. This theoretical paper points to the critical importance of the Si-unbound oxygen site in the process of hole and electron capture in oxyorthosilicates, which requires experimental verification.

In a recent review paper [22], we have already reported preliminary results on hole centers created at oxygen anions in YSO. The present paper is focused on clarification of the

nature of charge trapping centers in YSO crystals using both the conventional continuous wave (CW) and advanced pulse ESR techniques together with *in situ* x-ray irradiation of single crystals at cryogenic temperatures where created centers are thermally stable. The ESR data are compared with the TSL data obtained for the same crystals. Our results suggest that indeed both holes and electrons in YSO are preferably trapped at Si-unbound oxygen ions and their vacancies, respectively, confirming the theoretical prediction.

II. EXPERIMENTAL

Single crystals of YSO and LSO were grown from the melt by the Czochralski method in an argon atmosphere and using the iridium crucible in order to obtain the X2 polymorph [23,24]. Purity of raw materials was 4N. Electron spin resonance spectra indicate that the YSO crystal contained traces of Mo and P ions.

YSO and LSO crystallize in the monoclinic structure in the space group $C2/c$ [24], which is schematically shown in Fig. 1. The lattice is constructed from the oxygen tetrahedra with Si in the center. There are two crystallographically different Y/Lu sites with seven or six neighboring oxygen ions. The large spheres in Fig. 1 represent Si-unbound oxygen ions, which are surrounded by four Y ions.

For EPR measurements, crystals were cut in three orthogonal planes (a^*b), (bc), and (a^*c). The axis a^* was deflected from the crystallographic axis a by an angle of $32°$ in order to satisfy the orthogonality between crystal planes.

Continuous wave ESR measurements were performed at 9.25–9.8 GHz with the standard 3 cm wavelength of the ESR spectrometer in the 10–200 K temperature range using an Oxford Instrument cryostat. Crystals were x-ray irradiated directly in the spectrometer cavity at temperatures of 10–30 K. The pulsed ESR experiments were carried out with a Bruker E580 spectrometer with a dielectric resonator including the electron spin echo envelope modulation (ESEEM) and hyperfine sublevel correlation spectroscopy (HYSCORE) pulse techniques.

For the TSL study, the crystal was x-ray irradiated at 4.2 K in a liquid helium cryostat. The TSL glow curves were measured in the 4.2–290 K temperature range with the heating rate of 0.1 K/s. The needed TSL spectrum range was
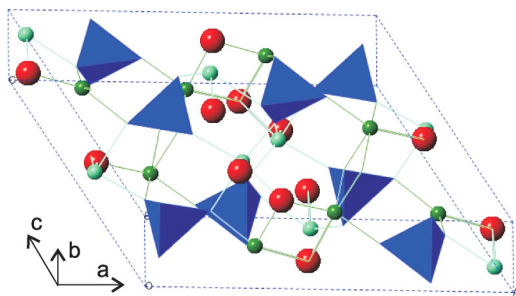
separated by optical filters. The TSL intensity was detected by a photomultiplier with an amplifier and recorder.

III. EXPERIMENTAL RESULTS AND DISCUSSION

The obtained experimental results are presented in the following order. First, the data on the paramagnetic centers created in YSO crystals under x-ray irradiation at room temperature are presented. The ESR spectra from the trapped hole and trapped electron (TE) centers, created by irradiation below 20 K, are considered in the second subsection. The thermal stability of different paramagnetic centers and their comparison with TSL data are presented in the third subsection. In the final part, proposed models of the trapped hole and electron centers are described, and the situation with x-ray induced centers in LSO crystals is discussed. In the Appendix, we present the results of the pulse ESR and HYSCORE of hole centers used to resolve weak HF couplings.

A. X-ray irradiation at room temperature

Before x-ray irradiation, YSO crystals contained weak ESR signals from unidentified impurities [Fig. 2, spectrum (a)]. After x-ray irradiation at room temperature (40 kV, 10 mA, 30 min), an intense ESR spectrum appears [Fig. 2(b)]. The analysis shows that the spectral lines with resonances at 370 and 340 mT belong to two different Mo centers, $Mo^{5+}(I)$ and $Mo^{5+}(II)$, while the spectrum in the lower magnetic fields belongs to O^- ions described by us in Ref. [22].

1. Mo^{5+} centers

Mo centers were easily identified due to the observation of the well-resolved HF lines originating from two $^{95,97}Mo$ isotopes with $I = 5/2$ nuclear spins of almost equal magnetic moments. Thus, the individual HF lines from the different isotopes are not resolved. The total natural abundance of these two isotopes is 25.2%. Two Mo centers differ essentially by linewidths of the spectral lines and spin-lattice relaxation times. Due to a short spin-lattice relaxation time, the Mo(I)

FIG. 1. (Color online) The crystal structure of X2-Y(or Lu)$_2$SiO$_5$. Blue tetrahedra represent (SiO$_4$)$^{4-}$ units; the small dark green and light blue spheres represent the two crystallographically different Y (or Lu) sites and the large red spheres are Si-unbound oxygen ions.
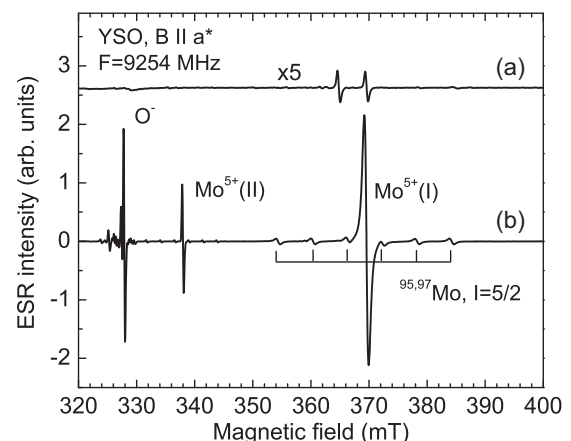

FIG. 2. ESR spectrum of the YSO single crystal measured before (a) and after (b) x-ray irradiation at room temperature. The spectra are taken at 30 K at the orientation $B \parallel a^*$. Strong ESR lines from the Mo^{5+} and O^- centers are identified.
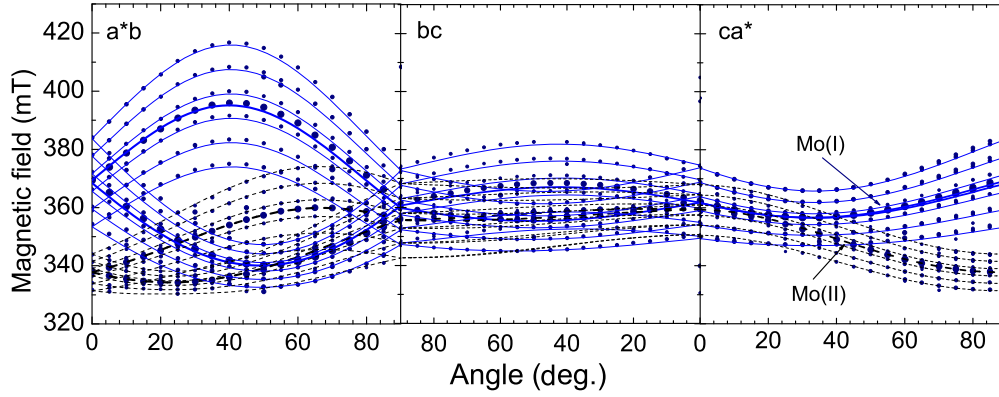
FIG. 3. (Color online) Angular dependencies of Mo^{5+} resonance fields measured in the (a^*b), (bc), and (ca^*) planes. Discrete symbols are the experimental data (the size of symbols is proportional to the intensities of the spectral line); the solid blue and dashed black lines are calculated data for the $Mo^{5+}(I)$ and $Mo^{5+}(II)$ centers, respectively. The calculated HF resonances are shown by thin blue and black lines.

center can be measured only at $T < 50$ K, while the Mo(II) center, having considerably longer spin-lattice relaxation time, can be measured starting from approximately 150 K. In order to confirm the charge state of the Mo ions responsible for the two Mo centers and to determine the spin Hamiltonian parameters, the angular dependencies of Mo resonance lines were measured in three perpendicular planes: (a^*c), (a^*b), and (bc). The experimental data together with the calculated data are shown in Fig. 3. One can see that the spectral lines split in two components when the magnetic field deviates from the crystal axes, suggesting existence of two magnetically nonequivalent positions for the paramagnetic ion in each center, which differ in orientation of g tensor principal axes.

The measured angular dependencies of the Mo resonance fields are well fitted by the spin Hamiltonian for a paramagnetic particle with the electron spin $S = 1/2$ and nuclear spin $I = 5/2$ for both ^{95,97}Mo isotopes. The g tensor and HF tensor parameters determined from the fit of the measured angular dependencies averaged for two Mo isotopes are presented in Table I. g factor values (1.70–1.98) and HF splittings determined for both centers are typical for Mo^{5+} ($4d^1$) ions [25]. This is also confirmed by measurements at the microwave frequency 34 GHz, where the spectra were described by the same g factor values as at 9.25 GHz. Let us analyze these spectral parameters.

The low-symmetry crystal field of the YSO lattice lifts all orbital degeneracy of the $4d^1$ orbitals. For a d^1 ion, a g value of ~ 2, as found for Mo(II) ($g_z = 1.978$), occurs only if the unpaired electron occupies a $|3z^2 - r^2\rangle$ orbital. The other two principal g factors will be shifted from 2.0023 to first order by

$$\Delta g_x = -\frac{6k\lambda}{E_{yz}}; \Delta g_y = -\frac{6k\lambda}{E_{xz}}, \quad (1)$$

where $\lambda \approx 1000$ cm^{-1} is the spin-orbit coupling constant of a Mo^{5+} ion and E_{yz} and E_{xz} are the energy differences between the ground state and the yz and xz orbitals, respectively. k is the spin-orbit coupling reduction factor. With $k \approx 0.7$, Eq. (1) gives $E_{yz} = 26\,000$ cm^{-1}, $E_{xz} = 12\,200$ cm^{-1}, and $E_{yz} = 24\,800$ cm^{-1}, $E_{xz} = 26\,500$ cm^{-1} for the Mo(I) and Mo(II) centers, respectively, which are quite reasonable values as for a Mo^{5+} ion. In the pure $3z^2 - r^2$ ground state, Δg_z should be very

small. The nonzero Δg_z is usually explained by the mixing of $x^2 - y^2$ orbital in the ground state [26]. The corresponding expression, to first order, depends on the separation between the ground state and the excited state $|xy\rangle$ and the mixing coefficient α:

$$\Delta g_z = -8\alpha^2 \frac{k\lambda}{E_{xy}}. \quad (2)$$

The mixing coefficient α can be determined from analysis of HF parameters. We use the formulas derived in Ref. [27] for Ti^{3+} ions on Sr^{2+} sites in $SrTiO_3$. The principal values of the HF coupling tensor are

$$
\begin{aligned}
A_z &= A + P\left[\frac{4}{7} - \frac{1}{14}\left(\Delta g_x + \Delta g_y\right)\right], \\
A_x &= A + P\left(-\frac{2}{7} + \Delta g_x - \frac{1}{14}\Delta g_y - \frac{4}{7}\sqrt{3}\alpha\right), \\
A_y &= A + P\left(-\frac{2}{7} + \Delta g_y + \frac{1}{14}\Delta g_x + \frac{4}{7}\sqrt{3}\alpha\right), \\
\Delta g_i &= g_i - 2.0023.
\end{aligned}
\quad (3)
$$

A describes the contact HF interaction; $P = g g_n \beta \beta_n \langle r^{-3} \rangle_{3d}$, where g, g_n, β, and β_n are the electron and nuclear g factors and the Bohr and nuclear magnetons, respectively. Since the signs of A_i are unknown, a solution of the set of Eq. (3) is sought, which gives a reasonable value of P (P is negative) and the greatest value of $|A|$. Such a solution is obtained with $A_i > 0$. Comparison of Eq. (3) with the experimental parameters then leads to $A = (121 \pm 5)$ MHz, $P = -(74 \pm 2)$ MHz, $\alpha = -0.5 \pm 0.1$ for the Mo(I) center and $A = (86 \pm 5)$ MHz, $P = -(75 \pm 1)$ MHz, $\alpha = -0.38 \pm 0.05$ for the Mo(II) center. By using the determined isotropic contact term A, the parameter [28]

$$\chi = \frac{4\pi}{S}\left(\psi \left| \sum_i \delta\left(r_i\right) s_{zi} \right| \psi\right) = -\frac{3}{2}\left(\frac{hca_0^3}{2.0023 g_n \beta \beta_n}\right) A,$$

which characterizes the density of unpaired spin at the nucleus, can be calculated. Here $a_0 = 0.528$ cm^{-8} is the Bohr radius. This gives $\chi = -5.15$ and -3.64 for the Mo(I) and Mo(II) centers, respectively. These values are in a range obtained for Mo^{5+} in other crystals (see, e.g., Ref. [29]).

TABLE I. Spectral characteristics of the hole and electron traps in the YSO crystals obtained from the ESR data. The principal axis directions of g and HF tensors are given by polar (θ) and azimuthal (φ) angles relatively to the a^*, b, c crystal axes and are presented for one of two equivalent centers. The error margin of the polar and azimuthal angles is approximately 2–3°.

Center	g tensor	Principal axes		HF interaction	Principal axes	
		θ (deg.)	φ (deg.)		θ	φ
Mo^{5+}(I)	g_y: 1.657(2)	107	40	A_y(^{95,97}Mo): 211(3) MHz	Identical to	
	g_x: 1.842(2)	17	49	A_x(^{95,97}Mo): 107(3) MHz	g tensor	
	g_z: 1.944(2)	92	131	A_z(^{95,97}Mo): 77(3) MHz		
Mo^{5+}(II)	g_y: 1.833(2)	128	66	A_y(^{95,97}Mo): 147(2) MHz	Identical to	
	g_x: 1.844(2)	38	68	A_x(^{95,97}Mo): 89(2) MHz	g tensor	
	g_z: 1.978(2)	89	337	A_z(^{95,97}Mo): 42(2) MHz		
O^- (STH)	g_x: 2.0127(5)	90	90	A(^{89}Y): ~9 MHz	not determ	
	g_y: 2.0115(5)	15	178			
	g_z: 2.0203(5)	75	360			
TE (F^+)	g_1: 1.9810(2)	353	14	A(^{89}Y): ~(25–30) MHz	not determ	
	g_2: 1.9877(2)	7	36			
	g_3: 1.9838(2)	31	335			
O^-(I)	g_x: 2.0124(2)	93	340	A_1(^{89}Y): 17.0(5) MHz	46	350
	g_y: 2.0100(2)	24	64	A_2(^{89}Y): 15.5(5) MHz	49	202
	g_z: 2.0038(2)	114	72	A_3(^{89}Y): 25.0(5) MHz	73	97
O^-(II)	g_x: 2.0037(2)	60	9	A_1(^{89}Y): 2.1 MHz [*]	not determ.	
	g_y: 2.0078(2)	104	91	A_2(^{89}Y): 0.88 MHz [*]		
	g_z: 2.0505(2)	33	159			

[*]HF constants at $\angle(B, a^*) = 45°$

Note that the value of P is significantly smaller than that predicted for an isolated Mo^{5+} ion, $P = -201$–204 MHz [29]. One would thus expect a value of P, corresponding to an oxidation state, considerably smaller than the formal valence 5+ due to the charge transfer in the bonding orbitals.

The absence of any other ESR signal from Mo suggests that before irradiation, Mo was in the nonparamagnetic Mo^{6+} state. Due to the relatively large ionic radius of Mo^{6+} (0.41 Å) with respect to the ionic radius of Si^{4+} (0.26 Å) in the fourfold oxygen coordination [30], we assume that the Mo^{6+} ions substitute for Y^{3+} ions, whose ionic radius (0.90–0.96 Å) is larger than the ionic radius of $Mo^{6+/5+}$ (0.59–0.73 Å) for the oxygen coordination numbers of 6–7 of YSO lattice [24]. Both Y lattice sites have the C_1 symmetry. It cannot be excluded that at least one of the Mo centers is associated with Y vacancies in order to compensate for the excess charge introduced by Mo^{6+} ions.

Note that g and HF tensor axes of both Mo^{5+} centers are not related to any characteristic crystal direction due to low crystal symmetry of YSO and local relaxation of the lattice when Y ions are replaced by the smaller Mo ions. In this situation, probably only DFT-based simulation can clarify actual structure of these centers.

Both Mo^{5+} centers created under the x-ray irradiation are thermally stable up to approximately 490 K. At these temperatures, Mo^{5+} ion loses an electron and becomes transformed into Mo^{6+} as confirmed by TSL measurements [31].

2. O$^-$- type centers

After x-ray irradiation of the YSO crystal at room temperature, together with the Mo^{5+} spectra, other resonances arise in the magnetic field range of 324–330 mT. These magnetic fields correspond to the resonances of hole-type paramagnetic particles usually having g factors larger than $g = 2.0023$ [32]. As it was shown in our preliminary study [22], the resonances at 324–330 mT originate from the Si-unbound oxygen ions, which have trapped a hole under x-ray irradiation and become the O^- ($2p^5$, $S = 1/2$) paramagnetic ions. Depending on the heating duration at room temperature, at least two different O^- centers were distinguished, denoted as O^-(I) and O^-(II).

The resonance lines are very narrow. The peak-to-peak linewidth is approximately 0.03 mT. The narrowness of the linewidths allows us to resolve the HF structure of the resonance lines. This structure is well visible in spin-echo-detected electron paramagnetic resonance (ED EPR) shown in Fig. 4 for the O^-(I) center.
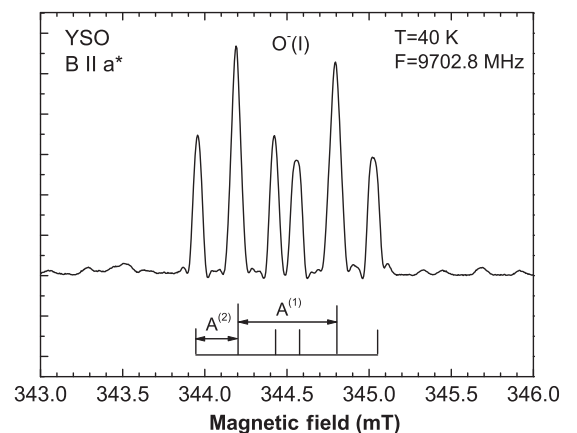

FIG. 4. Spin-echo-detected EPR spectrum of the O^-(I) center created by the x-ray irradiation at room temperature. The spectrum has a pronounced HF structure composed of two triplets.

There are two HF triplets with an intensity ratio 1:2:1. The large splitting $A^{(1)}$ is due to one nucleus with a 1/2 nuclear spin and of 100% abundance. The small splitting $A^{(2)}$ is produced by two nearly equivalent nuclei with the same 1/2 spin and 100% abundance. The ESR line of the O^-(II) center is split only into three components with an intensity ratio 1:2:1. Therefore, it is reasonable to assume that the HF triplets are produced by two equivalent ^{89}Y lattice nuclei, which have the nuclear spin 1/2, natural abundance 100%, and small nuclear g factor, $g_n = -0.2736$, while the large splitting in the O^-(I) center is produced by nucleus with a much larger magnetic moment.

In order to complete our study of the O^- centers and determine g and HF parameters, we measured angular dependencies of the resonance lines for both hole centers in three perpendicular planes, as was done for Mo centers. The results are shown in Figs. 5 and 6. Both hole centers have two magnetically inequivalent positions in the lattice for the O^- ion, in accordance with the space group $C2/c$ of the crystal.

The angular dependencies of the O^-(I) center were fitted by the spin Hamiltonian for a paramagnetic particle with the electron spin 1/2, taking into account only larger HF interaction with one $I = 1/2$ nucleus. g and HF parameters of the spin Hamiltonian are presented in Table I. For the O^-(II) center, only the electron Zeeman term was included into the spin Hamiltonian since HF splitting is weak and poorly resolved for all angles. g tensor parameters of the O^-(II) center are also presented in Table I. It can be noticed that g factors of both hole centers are typical for O^- ions [25,32].

The g factors of the O^-(I) center can be reasonably interpreted assuming that the unpaired electron moves in a p_z orbital of the p^5 state of the O^- ion. The angular momentum is quenched in this state (the corresponding g factor is close to the free spin value), and the deviations of the other two g values from the free spin value are due to the admixture of p_x and p_y orbitals into the ground state by spin-orbit coupling [33]:

$$\Delta g_i = -\frac{2\lambda}{E_i}, \quad i = x, y, \qquad (4)$$

where $\lambda \approx -150$ cm^{-1} is the O^- spin-orbit coupling constant, and E_i are the energy separations of the higher p states from p_z. By using Eq. (4), one derives with the observed g_x and g_y, $E_x = 30\,000$ cm^{-1} and $E_y = 39\,000$ cm^{-1}. For the second,

O^-(II) center, by assuming a p_z orbital as a ground state, one derives $E_x = 6200$ cm^{-1} and $E_y = 55000$ cm^{-1}, indicating a huge rhombic distortion of this center.

The important piece of information is taken from the values of the HF parameters of the O^-(I) center, namely from the $A^{(1)}$ HF interaction, which seems to be much stronger than expected for an ^{89}Y nucleus. The HF tensor is nearly axially symmetric around its z axis (see Table I). All components of the HF tensor have the same sign. Only under this assumption the HF structure of the spectrum can be reproduced by a theoretical simulation. Decomposing A into its isotropic (a), axial (b), and rhombic (e) parts

$$
\begin{aligned}
A_z &= a + 2b, \\
A_x &= a - b + e, \\
A_y &= a - b - e,
\end{aligned}
\qquad (5)
$$

one arrives at $|a| = 6.4, |b| = 0.94, |e| = 0.26 \times 10^{-4}$ cm^{-1}. Since the dipole-dipole coupling between magnetic moments of a nucleus and the unpaired electron of an O^- ion determines the magnitude of the axial HF interaction parameter, b, one can check whether the ^{89}Y nucleus is responsible for the b value. Taking, as a boundary case, the situation when the O^- orbital shrinks to a point, we have

$$b = \frac{\mu_0}{4\pi} g\beta g_n \beta_n \langle R^{-3} \rangle, \qquad (6)$$

where R is the distance between the nucleus and the O^- site. Comparison with the experimental b value yields $R = 0.12$ nm for the ^{89}Y nucleus, which is ~55% of the shortest distance expected for an undistorted lattice, 0.216 nm. This fact suggests that the nucleus with much bigger magnetic moment is responsible for the HF interaction described by the $A^{(1)}$ tensor. All criteria (the nuclear spin 1/2, 100% abundance, large magnetic moment) satisfy only ^{31}P. It gives $R = 0.225$ nm, which agrees well with the average distance between the Si-unbound oxygen ion and Y ions, 0.223 nm. We thus conclude that one of the Y^{3+} ions in the close vicinity of the O^- ion is replaced by a P^{3+} or P^{5+} ion. This impurity could be penetrated into the crystal with raw materials, most probably with Si, which usually contains some amount of P ions. We will discuss more the models of both O^- centers in Sec. III D.
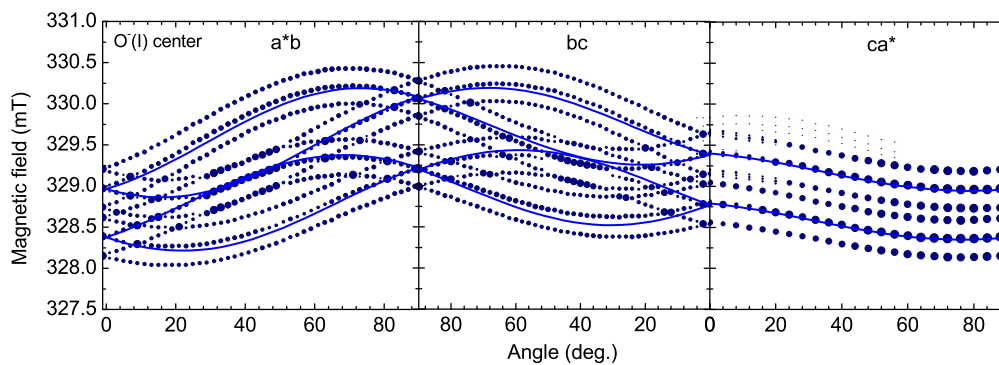

FIG. 5. (Color online) Angular dependencies of O^-(I) resonance fields measured in the (a^*b), (bc), and (ca^*) planes. The discrete symbols are the experimental data, and solid lines are the calculated data. The fit is done only for the larger HF splitting with the HF constants listed in Table I.
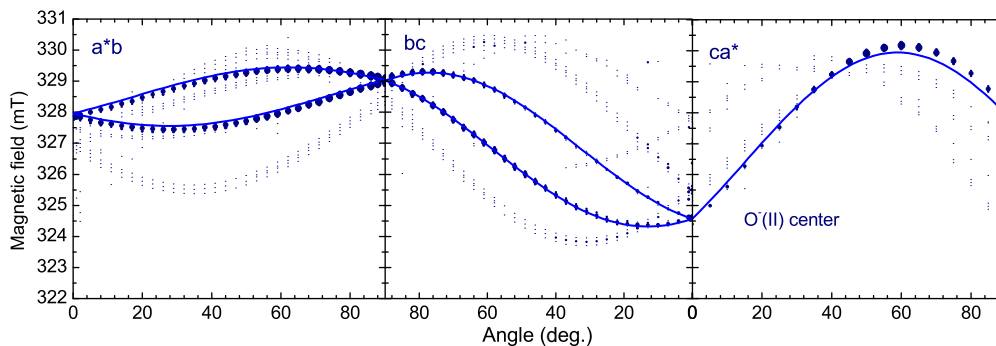
FIG. 6. (Color online) Angular dependencies of O$^-$(II) resonance fields measured in the (a^*b), (bc), and (ca^*) planes. The discrete symbols are the experimental data and solid lines are the calculated data. The fit is done only for the electron Zeeman interaction described by the spin $S = 1/2$. Other weak resonances, visible in the angular dependencies but not analyzed, also belong to O$^-$ ions with another surroundings than in the O$^-$(I) or O$^-$(II) centers.

B. X-ray irradiation at 20 K

1. STH center

The spectrum shown in Fig. 7 is created under x-ray irradiation at the temperature of approximately 20 K. The strong complex line at lower magnetic fields in Fig. 7 was identified previously [22] as that belonging to the STH center. It is broadened by saturation effects (long spin-lattice relaxation time) at the temperature of 55 K, which is nevertheless the most appropriate for the observation of the second spectrum at higher magnetic fields.

The spectrum of the STH is composed of five equidistant HF lines with the intensity ratio of 1:4:6:4:1 (for details, see Ref. [22]). This HF structure originates from the interaction of a paramagnetic particle with four nearly equivalent ^{89}Y nuclei. The angular dependencies of the resonance fields of
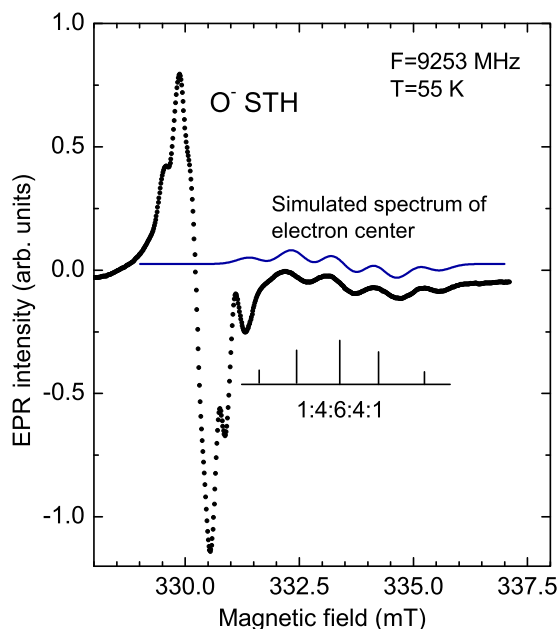

FIG. 7. (Color online) ESR spectrum created by x-ray irradiation of YSO at 20 K. The strong line at $\approx$330 mT belongs to a trapped hole center; the second line at $\approx$333.5 mT with HF structure belongs to a trapped electron center. The spectrum is measured at $B \parallel c$. The simulated spectrum of a trapped electron center is shown as well.

this spectrum (Fig. 8) are described by the spin Hamiltonian for the paramagnetic particle with the spin $S = 1/2$ containing only electron Zeeman term, as the ^{89}Y HF splitting is too weak to be well resolved at all angles. We also neglect the small splitting of resonance lines corresponding to two magnetically nonequivalent positions of the paramagnetic ion. The calculated g factors are listed in Table I. These g factors are larger than the g factor of a free electron. It confirms that the created spectrum belongs to a trapped hole center. During the heating of the irradiated crystal up to approximately 140–160 K, the spectrum of the STH center transforms into the spectrum of the O$^-$(I) center. We assume that the hole spectrum created by x-ray irradiation at low temperatures belongs to the STHs at the Si-unbound O5 ions. This assumption agrees well with the HF structure, which shows that the trapped hole interacts with four Y nuclei. The model of the center is confirmed by other experimental data considered below.

2. g tensors and HF interactions of the STH center

In the analysis of the g tensor of the STH center, we take into account that one of the g tensor components ($g_y = 2.0015$) is smaller of the free electron value 2.0023. It suggests that a trapped hole occupies the p_x or p_y orbital of the $2p_\pi$ ground state of an O$^-$ ion. For the $2p_\pi$ ground state, the g factors can be described by the following expressions previously introduced for the O$_2^-$ molecule in alkali halides [34], which have the same p_π ground state:

$$g_x = g_e \cos\vartheta - g_l \left(\frac{\lambda}{D}\right)(\cos\vartheta + 1 - \sin\vartheta), \quad (7a)$$

$$g_y = g_e \cos\vartheta - g_l \left(\frac{\lambda}{D}\right)(\cos\vartheta - 1 + \sin\vartheta), \quad (7b)$$

$$g_z = g_e + 2g_l \sin\vartheta, \quad (7c)$$

with $\sin\vartheta = \lambda/2E$ and $g_e = 2.0023$. Here D is the distance from the ground state to the highest p_σ orbital in the hole representation, E is the splitting of the twofold degenerate p_π orbital, and g_l is the O$^-$ orbital g factor. Taking $g_l = 1$ as for the free O$^-$ ion, one can determine the following splitting of $2p$ orbitals: $D = 29000$ cm^{-1} and $E = 8300$ cm^{-1}.
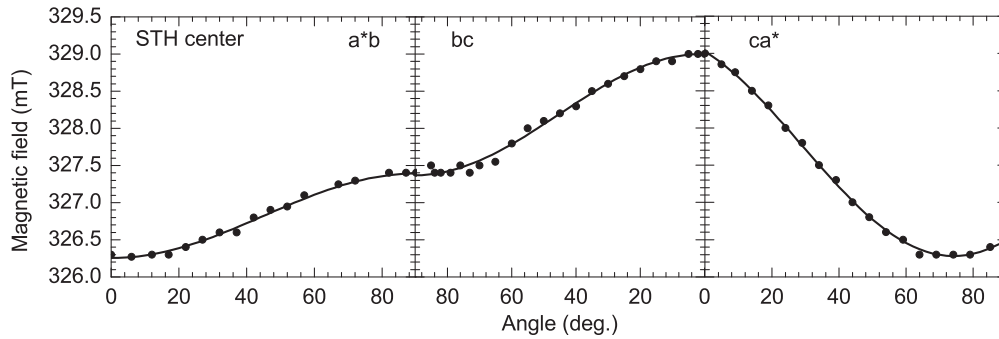
FIG. 8. Angular dependencies of the O$^-$ STH center resonance fields measured in the (a^*b), (bc), and (ca^*) planes. The discrete symbols are the experimental points, and the solid lines are the calculated data. The fit is carried out assuming only the electron Zeeman interaction for the spin $S = 1/2$.

3. TE center

We assume that the line with the resolved HF structure in higher magnetic fields shown in Fig. 7 belongs to the trapped electron center. The HF structure consists of five components with the intensity ratio 1:4:6:4:1. It arises from the interaction of an electron spin with nuclear magnetic moments of four nearly equivalent ^{89}Y nuclei like in the STH center. The HF interaction is slightly anisotropic, and the corresponding HF splitting ranges from 0.9 to 1.1 mT. Besides, the center has two magnetically nonequivalent positions in the lattice like other paramagnetic centers in YSO. However, the separation between the corresponding spectra is so small that it can hardly be measured. Therefore, the resonance fields of the TE center presented in Fig. 9 were measured as the center of gravity of the two spectra. The angular dependencies were described by the spin Hamiltonian for a paramagnetic particle with the spin $S = 1/2$, taking into account only the electron Zeeman term, as the ^{89}Y HF splitting is not well resolved at all angles. The determined g factors are presented in Table I. These g factors are smaller than the g factor of a free electron. It suggests that the spectrum belongs to the TE center.

The HF structure of the TE center indicates that electron density is distributed over four Y ions around of the Si-unbound oxygen O5 site. Therefore, the TE center can be assigned to the F$^+$ center created at the Si-unbound oxygen vacancy. The negative g factor shift can be naturally explained in the linear combination of atomic orbitals (LCAO) approximation by considering the wave function of the F$^+$

electron as a linear combination of the wave functions of the four nearest Y neighbors. In other words, the TE will partly occupy the $4d^1$ orbital of each nearest Y neighbor. In this case, the g factor shift will depend on the T_{2g}-E_g splitting of the $4d^1$ orbital levels, assuming the E_g doublet to be the ground state. Only this ground state can explain the small g factor shift of the F$^+$ center, $\Delta g = 0.015$–0.021. We can thus apply the same expressions (1–2) used in the analysis of the Mo^{5+} spectra. Taking the spin-orbit coupling constant $\lambda \approx 290$ cm^{-1} and, for instance, the energy of the T_{2g}-E_g splitting 32 000 cm^{-1}, the measured g factor shifts can by obtained with the spin-orbit coupling reduction factor $k \approx 0.4$. Here the coefficient k roughly characterizes the normalized spin density of F$^+$ electron at the Y ion.

In principle, the HF structure also provides information on the electron density distribution. For the TE center, the HF interaction is predominantly isotropic, of Fermi contact type. Its value can be theoretically estimated from the HF interaction of the free Y atom, a_{at}, and the s-wave character of the LCAO approximation, ξ, as [35]

$$a_{IF} = \tfrac{1}{4}\xi \cdot a_{at}, \qquad (8)$$

where the coefficient 1/4 accounts for the distribution of F$^+$ electron density over the four nearest-neighboring Y ions. Taking $a_{at} = -19.1 \times 10^{-4}$ cm^{-1} as for the free Y atom [36], and even $\xi = 1$, Eq. (8) gives only 1/2 of the measured HF splitting, which is $\approx 10 \times 10^{-4}$ cm^{-1}. So, one can see that while the simple LCAO approximation in general provides
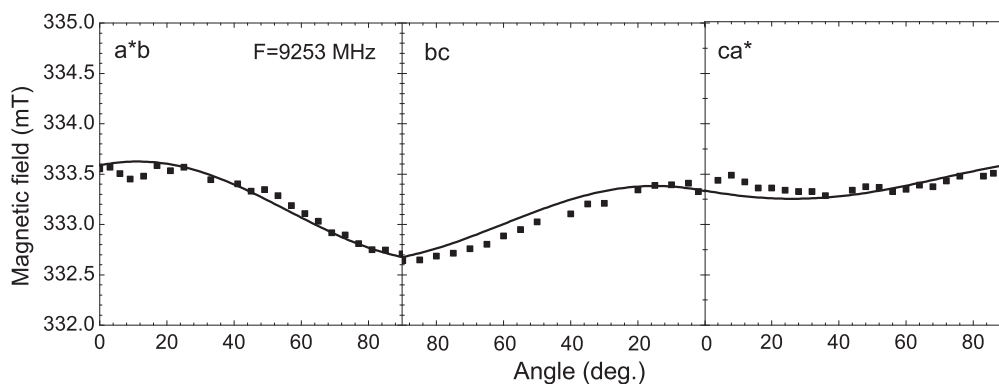

FIG. 9. Angular dependencies of the TE center resonance fields measured in the (a^*b), (bc), and (ca^*) planes. The solid lines are the calculated data. The fit is carried out assuming only the electron Zeeman interaction for the spin $S = 1/2$.

a qualitative agreement with the experiment, the quantitative agreement in HF interaction is far from to be satisfied.

C. Thermal stability of electron and hole trapping centers and correlation with TSL data

The thermal stability of the x-ray created centers was studied by the pulse heating method. After irradiation at the selected temperature T_{irr}, the sample was heated at a rate of 1–2 K/s up to a certain temperature T_{an}, held at that temperature for 3 minutes and then quickly cooled down (with a rate of 4 K/s) to a fixed temperature where the ESR intensity was measured. Except for the irradiation, which was carried out only once during the first step, this procedure was repeated for different temperatures T_{an}. The 3 minute interval was determined as the optimum balance between good thermalization of the sample and sufficient reproducibility of the measured ESR intensities. The signal amplitudes obtained in such a way are depicted in Fig. 10, which presents the data on ESR intensity as the function of the annealing temperature together with the TSL data obtained for the same crystal for the (290–360) nm emission. It can be seen that the STH ESR spectrum shows constant intensity up to 75 K and only partial decrease at $T > 75$ K. At the same time, the concentration of electron centers abruptly decreases at 75 K up to complete disappearance of their spectrum due to the thermal ionization of the TEs. Therefore, the complex TSL glow curve peak at 75–90 K can be assigned to the recombination of thermally released electrons at hole-related centers. This can be seen also in a slight decrease of the number of STHs at 80 K whose concentration is much higher than the concentration of TE centers. A further decrease in the TSL intensity at higher temperatures (90–130 K) is caused by the thermal delocalization of STHs whose concentration (the ESR intensity) declines similarly. A fraction of the liberated holes are retrapped at other lattice sites, thus resulting in
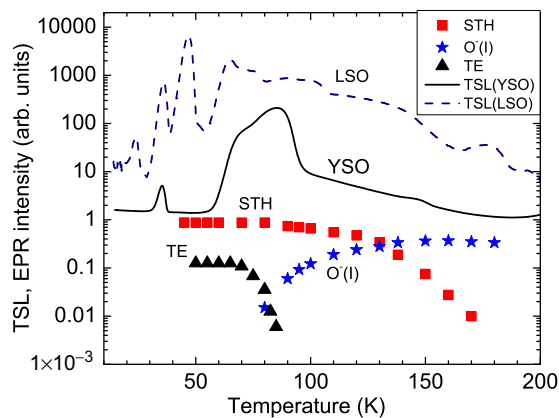

FIG. 10. (Color online) Dependence of ESR relative intensities of the TE, O$^-$ STH and O$^-$(I) centers on the temperature of pulsed annealing measured in the YSO crystal x-ray irradiated at 20 K. The data also show the transformation of the STH center into the O$^-$(I) center. The TSL glow curve measured for the same crystal is presented as well. For comparison, the figure shows the TSL glow curve of Lu$_2$SiO$_5$ obtained after x-ray irradiation at 4.2 K.
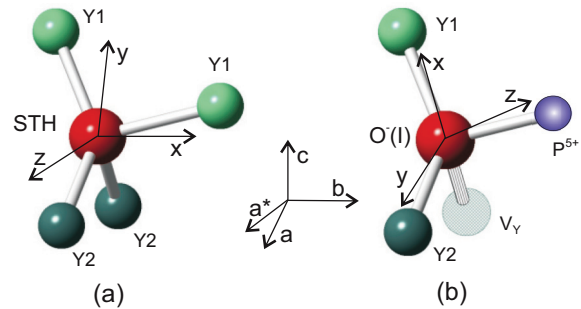

FIG. 11. (Color online) Models of two O$^-$ hole centers created by x-ray irradiation in YSO crystals: (a) STH center; (b) O$^-$(I) center. In the O$^-$(I) center one of the four Y ions is missing, and the second Y ion is replaced by a P^{5+} impurity ion. x, y, and z axes are the g tensor principal axes for one of two equivalent positions of each center. Their polar and azimuthal angles are presented in Table I.

the formation of O$^-$(I) centers whose concentration begins to increase at 80 K and saturates at 130–150 K.

For comparison, we also present in Fig. 10 a TSL glow curve for LSO measured at the same experimental conditions. LSO is isostructural crystal to YSO and is characterized by practically the same unit cell parameters as YSO. However, one can see that TSL curves in the both crystals are essentially different. In particular, the strong peak at 70–90 K visible in YSO, which is related to the thermal release of TEs, is almost suppressed in LSO. Note that while Ref. [14] reports the observation of ESR spectrum of F$^+$ center in powdered LSO samples, we were not successful in detection of any x-ray induced spectra in our LSO crystals; even Mo^{5+} centers were hardly be observed. This does not allow us to discuss possible origin of TSL peaks in LSO based on ESR data. Systematic analysis of the TSL glow curves in both undoped and Ce-doped YSO and LSO crystals based on separate study of the electron (Ce^{3+}-, Tb^{3+}-related) and hole (Sm^{3+}-, Eu^{3+}-related) recombination luminescence presented by us in Ref. [31] confirms the conclusions on the electron or hole origin of the paramagnetic centers detected in the present work.

D. Models of hole and electron trapping centers

1. Trapped hole centers

All hole centers observed by us are related to oxygen lattice ions. There are five different crystallographic sites for lattice oxygen ions in the YSO structure [23,24]. Four oxygen ions (O1–O4) are bound only with Si ions, thus forming isolated SiO$_4$ tetrahedra. The fifth Si-unbound oxygen ion (O5) is surrounded by four Y ions. Since no ^{29}Si HF interaction was resolved even by the ESEEM technique (see Appendix), it is likely that a hole is trapped at the Si-unbound oxygen O5 ion. This hypothesis is also supported by the observation of the well-resolved HF structure produced by ^{89}Y nuclei with relatively strong HF interaction. The hole interacts with all four Y nuclei in the shallowest O$^-$ center. Therefore, the oxygen ion with a trapped hole is not markedly perturbed by a defect, and the hole is self-trapped at the oxygen ion [the STH center, Fig. 11(a)]. One of the g tensor principal axes of this center, corresponding to g_x, coincides with the b crystal axis. Two

other principal axes are turned by the angle 15° from the c crystal direction in the ac plane. In the other hole centers, the Si-unbound oxygen ion is clearly perturbed by a defect. It could obviously be a defect at the Y site, as the HF structure of the corresponding ESR spectra indicates that the unpaired electron interacts only with two [89]Y nuclei. Therefore, two Y ions are missing in the OY_4 tetrahedron [Fig. 11(b)]. In the $O^-(I)$ center, one of the Y neighboring ions is replaced by a P ion. Namely, the O^- p_z orbital is oriented approximately along the O-P direction. The ^{31}P HF interaction is also stronger along this direction. We suppose that the second Y neighboring site is vacant, and the P ion has its normal valence state 5+, which makes the center to be charge compensated. Of course, these graphical models only roughly reflect real configuration of the hole defects. In particular, the difficulty in the g tensor interpretation is related to the C_1 symmetry of the oxygen O5 site and complex distortion of the Y_4O unit, whose shape is far from the ideal tetrahedron.

Possible candidates for the defective sites in the $O^-(II)$ center are an yttrium vacancy (V_Y) and a Mo ion. The incorporation of Mo ions into the YSO lattice is confirmed directly by the measurements of Mo^{5+} ESR spectra. The high valence state of the molybdenum suggests that the YSO crystals contain yttrium vacancies. Each Mo^{6+} ion can evidently compensate for the negative charge of one yttrium vacancy. It is also reasonable to assume that before x-ray irradiation, the charge state of molybdenum is nonparamagnetic 6+; thus, the molybdenum also serves as an effective trapping site for electrons. Probably, due to the large concentration of such electron traps, the concentration of hole O^- centers is also relatively large in YSO crystals containing Mo ions. This fact is in line with the absence of O^- spectra in LSO crystals where Mo^{5+} ions are present in much lower concentration.

2. The TE center

The ESR spectrum of the TE center was convincingly enough assigned to the F^+ center created at the Si-unbound oxygen vacancy on the base of HF structure and g-factor analysis. However, the low thermal stability of the TE center, which becomes thermally ionized already at approximately 70–80 K, is rather atypical for complex oxides in which these centers were found to be stable even above room temperature [37,38]. For example, in Al_2O_3, the F^+ center survives up to 700 K [39]. Besides, DFT calculations for the isostructural LSO [21] show that the local electronic level of the 2+ state V_{O5} vacancy is located at 2.5 eV below the conduction band minimum. Bond energy of an electron at the oxygen vacancy should be lower by 0.5–1 eV. Even taking into account the quantitative uncertainties of the DFT calculation, the low thermal stability of the TE center (0.24 eV, as determined from TSL data [31]) is far from the predicted value 1.5–2 eV. Presently we can hardly resolve this contradiction. One of the possible explanations is that the 0.24 eV barrier is the activation energy for recombination in close {TE − hole center} pairs that take place without release of electrons from the TE center into the conduction band. This is in line with the TSL experiment [31].

3. X-ray induced ESR spectra in LSO

The presence of similar electron and hole traps can be, in principle, expected in LSO crystals due to the same crystallographic and chemical characteristics of both orthosilicates. However, no corresponding ESR spectra were convincingly detected by us in the studied LSO crystals or even in their powders. It can be an indication of lower concentration of electron and hole traps in LSO. For example, Mo concentration was found to be near detection sensitivity. However, it seems that the main reason of invisibility of the spectra of electron and hole traps could be a much stronger HF interaction of the electron spin with the nuclear magnetic moment of [175]Lu isotope, which has the nuclear spin of 7/2, large nuclear magnetic moment and quadrupole moment. Therefore, the ESR spectra in LSO are expected to be much wider as compared with YSO. In general, the spectral intensity will be distributed among a large number of HF lines, leading to decrease in intensity of each HF component. The number of only allowed transitions can be up to $N = \prod_{k=1}^{4} (2I_k + 1) = 4096$ for four Lu nuclei. Consequently, this essentially complicates the detection of resonance lines.

Note that recent studies of undoped YSO and LSO crystals allowed the suggestion that the oxygen-vacancy-related electron centers and O^--type hole centers considered in the present work take part in the tunneling and/or thermally stimulated recombination processes accompanied with the intrinsic visible emission of these crystals [40]. It was also found that these processes give a considerable contribution into the slow (ms-s) photoluminescence decay [40], afterglow, and TSL [41] of not only the undoped but also of the Ce-doped YSO and LSO crystals known as prospective scintillation materials.

IV. CONCLUSIONS

Detailed ESR investigation of the YSO single crystals x-ray irradiated at different temperatures has shown that the holes created by irradiation at $T < 80$ K are first self-trapped at Si-unbound oxygen ions forming O^- paramagnetic centers. At $T > 80$ K, the self-trapped holes become thermally delocalized and then retrapped at other Si-unbound oxygen ions with perturbing defects (e.g., yttrium vacancies, accidental impurity ions such as P, Mo ions, substituting for Y^{3+} ions, etc.) in their surroundings, which stabilize more deeply the trapped holes at the oxygen ions. As a result, a variety of O^- centers can be created with the thermal stabilities up to room temperatures or even higher. Two of such O^- centers can be ascribed to $O^- - V_Y - P_Y$ and $O^- - V_Y - Mo_Y$ complex defects containing an yttrium vacancy V_Y near an impurity ion. The ESR parameters of all the O^- centers studied are determined. In particular, the ESR spectra of all the O^- centers show the HF structure originating from the interaction of electron spins with the nuclear magnetic moments of neighboring [89]Y nuclei.

Besides the O^- hole centers, x-ray irradiation at $T < 60$ K creates the electron-type center. This center is characterized by g factors in the 1.98–1.99 range. From the analysis of the HF structure of its ESR spectrum, we concluded that an electron is trapped at the Si-unbound O5 vacancy, thus forming an F^+-type center. The TEs are assumed to be thermally

liberated at 75–90 K without an excitation to the conduction band. The recombination of these electrons with O^--type hole centers is accompanied by thermally stimulated intrinsic visible luminescence.

We found that Mo^{6+} impurity ions can also act as effective traps for electrons in Y and possibly Lu orthosilicates. Two Mo^{5+} centers were revealed in x-ray irradiated crystals, which were attributed to Mo at Y sites. The Mo^{5+} centers are thermally stable up to approximately 490 K. The release of electrons from Mo^{5+} is accompanied by the corresponding TSL peak [31]. In principle, Mo contamination is known for many scintillator crystals, for instance, for $YAlO_3$ [42], $Y_3Al_5O_{12}$ [43], and $Lu_3Al_5O_{12}$ [44]. Mo can penetrate from either the crucible or raw materials. As the iridium crucible was used to grow the YSO and LSO crystals studied, we assume that raw materials were the source of Mo contamination.

The identified intrinsic hole and electron centers in YSO structure point to critical importance of the Si-unbound oxygen site (O5) in the process of the hole and electron capture in oxyorthosilicates. Our results confirm also the preference of the tunneling mechanism in recombination processes of TEs and holes. It should stimulate further theoretical studies of this phenomenon as a common feature of oxyorthosiliocates.

APPENDIX: PULSE ESR AND HYSCORE OF O^- HOLE CENTERS

The ESEEM and HYSCORE pulse techniques are useful tools for resolving of small HF couplings of distant nuclei or nuclei with weak magnetic moments that cannot be resolved in the ordinary ESR spectra [45]. These techniques help to clarify the structure of a paramagnetic defect in many cases. The ESEEM spectrum for the O^-(I) center in the frequency domain is shown in Fig. 12. It was measured by the simple two-pulse spin-echo sequence $t_{\pi/2} - \tau - t_\pi - echo$. The spectrum is simple and contains the peaks attributed only to magnetic transitions of ^{89}Y nuclei. For the system with $S = 1/2$, $I = 1/2$, and isotropic or nearly isotropic HF interaction, these transitions appear at the frequencies [46]:

$$\nu_\alpha = \left| \frac{A}{2} + \nu_I \right|, \nu_\beta = \left| \frac{A}{2} - \nu_I \right|, \nu_+ = \left| \nu_\alpha + \nu_\beta \right|,$$

$$\nu_- = \left| \nu_\alpha - \nu_\beta \right|, \tag{A1}$$

where ν_I is the nuclear Larmor frequency.

In accordance with Eq. (A1), the peak at $\nu \cong \nu_I(^{89}Y) = 0.72$ MHz is produced by ^{89}Y nuclei distant from the O^- ion as the HF interaction is negligibly small ($A \cong 0$). The other two peaks located symmetrically around $\nu \cong \nu_I$ appearing at ν_α, ν_β frequencies are separated by the distance that corresponds
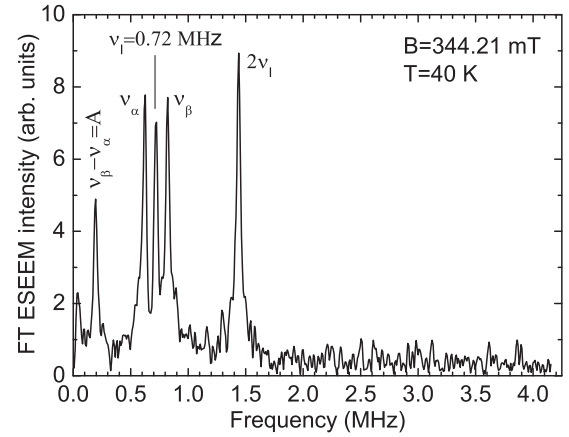

FIG. 12. Two-pulse FT ESEEM spectrum of the O^-(I) center measured at $B = 344.21$ mT; the crystal orientation $B \| a^*$ and a pulse sequence parameters $t_\pi = 140$ ns, $\tau = 1.6 \, \mu s$.

to a HF interaction $A = 0.19$ MHz. They are produced by the ^{89}Y nuclei located not far from the O^- ion. Also, these nuclei subsequently produce the peaks at $\nu_- = A = 0.19$ MHz and at $\nu_+ = 2\nu_I = 1.44$ MHz. No other nuclei are visible from the ESEEM spectrum. Thus, both the ESR and ESEEM spectra obviously show no impurity perturbing defect in the vicinity of the O^-(I) ion except for an yttrium vacancy and P ion.

The HF splitting in the ESR spectrum of the O^-(II) center is practically unresolvable due to weak HF interactions less than 0.1 mT. Therefore, the HYSCORE technique is useful for this center. The HYSCORE spectrum of the O^-(II) center for one of the crystal orientations is shown in Fig. 13.

The four-pulse sequence $t_{\pi/2} - \tau - t_{\pi/2} - t_1 - t_\pi - t_2 - t_{\pi/2} - echo$ used in this technique correlates the nuclear magnetic resonance transitions $\nu_{\alpha i}$ of one electron spin manifold M_α with the nuclear transitions $\nu_{\beta i}$ of the other electron spin manifold M_β. In case of single crystal spectra, the correlations appear in the two-dimensional spectrum as off-diagonal cross-peaks in the first order with frequencies at $([\nu_\alpha, \nu_\beta]; [\nu_\beta, \nu_\alpha])$ in the weak-coupling case ($A < 2\nu_I$) and at $([-\nu_\alpha, \nu_\beta]; [-\nu_\beta, \nu_\alpha])$ in the strong coupling case
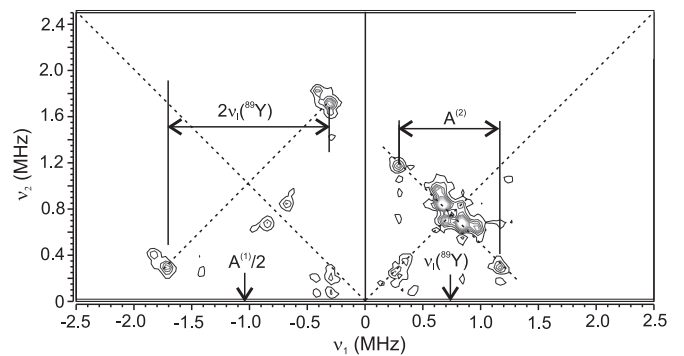

FIG. 13. The X-band HYSCORE spectrum measured in the YSO crystal in the resonance field ($B_0 = 343.39$ mT) of the O^-(II) center with different τ values at $T = 10$ K. The crystal orientation is $\angle(B, a^*) = 45°$.

($A > 2\nu_I$), which are symmetric with respect to the diagonal and antidiagonal lines, respectively. The frequencies ν_α, ν_β are directly related to the Larmor frequencies ν_I and HF coupling constants via, e.g., Eq. (A1) [45–46].

As shown in Fig. 13, there are two pairs of strong cross-peaks in the $(+, +)$ quadrant (weak coupling case) located at ([0.29, 1.17], [1.17, 0.29]) and ([0.67, 0.85], [0.85, 0.67]) MHz, which clearly relate to the HF interaction of holes with ^{89}Y nuclei. The lager HF constant $A^{(2)}$ is 0.88 MHz, while the smaller one is only 0.18 MHz.

In the $(-, +)$ quadrant (strong coupling case), there is only one pair of strong cross-peaks at ([-1.83, 0.40], [-0.40,

1.83]) MHz, which is attributed to the HF interaction of a hole with ^{89}Y nuclei. The corresponding HF constant $A^{(1)}$ is 2.1 MHz. These particular nuclei are responsible for the weak HF splitting of the O$^-$(II) EPR line (shown in fig. 10 of Ref. [22]). Except for ^{89}Y, no other nuclei were revealed in the HYSCORE spectrum. However, we cannot exclude that the group of cross-peaks at 0.6–1 MHz in the $(+, +)$ quadrant also contains resonances from the central transition $1/2 \leftrightarrow -1/2$ of ^{95,97}Mo nuclei as the nuclear Larmor frequencies of these two isotopes ($\nu_I \cong 0.9$ MHz) are close to the ^{89}Y Larmor frequency (0.73 MHz). The ^{95,97}Mo resonances can be simply lowered by the second order quadrupole effects [46].

[1] H. Suzuki, T. A. Tombrello, C. L. Melcher, and J. S. Schweizer, Nucl. Instrum. Methods Phys. Res., Sect. A **320**, 263 (1992).

[2] H. Suzuki, T. A. Tombrello, C. L. Melcher, and J. S. Schweitzer, IEEE Trans. Nucl. Sci. **40**, 380 (1993).

[3] D. W. Cooke, K. J. McClellan, B. L. Bennett, J. M. Roper, M. T. Whittaker, R. E. Muenchausen, and R. C. Sze, J. Appl. Phys. **88**, 7360 (2000).

[4] L. S. Qin, H. Y. Li, S. Lu, D. Z. Ding, and G. H. Ren, J. Cryst. Growth **281**, 518 (2005).

[5] H. Feng, V. Jary, E. Mihokova, D. Ding, M. Nikl, G. Ren, H. Li, S. Pan, A. Beitlerova, and R. Kucerkova, J. Appl. Phys. **108**, 033519 (2010).

[6] M. Balcerzyk, M. Moszynski, M. Kapusta, D. Wolski, J. Pawelke, and C. L. Melcher, IEEE Trans. Nucl. Sci. **47**, 1319 (2000).

[7] W. Drozdowski, A. J. Wojtowicz, D. Wiśniewski, P. Szupryczyński, S. Janus, J. L. Lefaucheur, and Z. Gou, J. Alloys Compd. **380**, 146 (2004).

[8] C. L. Melcher, M. A. Spurrier, L. Eriksson, M. Eriksson, M. Schmand, G. Givens, R. Terry, T. Homant, and R. Nutt, IEEE Trans. Nucl. Sci. **50**, 762 (2003).

[9] S. H. Shin, D. Y. Jeon, and K. S. Suh, Jpn. J. Appl. Phys., Part 1, **40**, 4715 (2001).

[10] T. Bottger, Y. Sun, G. J. Reinemer, and R. L. Cone, J. Lumin. **94–95**, 565 (2001).

[11] Y. K. Kuo, M. F. Huang, and M. Birnbaum, IEEE J. Quantum Electron. **31**, 657 (1995); C. Deka, B. H. T. Chai, Y. Shimony, X. X. Zhang, E. Munin, and M. Bass, Appl. Phys. Lett. **61**, 2141 (1992).

[12] F. Thibault, D. Pelenc, F. Druon, Y. Zaouter, M. Jacquemet, and P. Georges, Optical Lett. **31**, 1555 (2006).

[13] P. Dorenbos, C. W. E. van Eijk, A. J. J. Bos, and C. L. Melcher, J. Phys.: Condens. Matter **6**, 4167 (1994).

[14] D. W. Cooke, B. L. Bennett, R. E. Muenchausen, K. J. McClellan, J. M. Roper, and M. T. Whittaker, J. Appl. Phys. **86**, 5308 (1999); D. W. Cooke, M. W. Blair, J. F. Smith, B. L. Bennett, L. G. Jacobsohn, E. A. McKigney, and R. E. Muenchausen, IEEE Trans. Nucl. Sci. **55**, 1118 (2008).

[15] D. W. Cooke, B. L. Bennett, R. E. Muenchausen, J.-K. Lee, and M. A. Nastasi, J. Lumin. **106**, 125 (2004).

[16] L. Pidol, O. Guillot-Noel, A. Kahn-Harari, B. Viana, D. Pelenc, and D. Gourier, J. Phys. Chem. Solids **67**, 643 (2006).

[17] I. N. Kurkin and K. P. Chernov, Physica B **101**, 233 (1980).

[18] M. W. Blair, B. L. Bennett, S. C. Tornga, A. Smith, and R. E. Muenchansen, J. Appl. Phys. **108**, 104311 (2010).

[19] O. Guillot-Noël, Ph. Goldner, Y. L. Du, E. Baldit, P. Monnier, and K. Bencheikh, Phys. Rev. B **74**, 214409 (2006).

[20] W. Y. Ching, L. Ouyang, and Y.-N. Xu, Phys. Rev. B **67**, 245108 (2003).

[21] Bo Liu, Zeming Qi, Mu Gu, Xiaolin Liu, Shiming Huang, and Chen Ni, J. Phys.: Condens. Matter **19**, 436215 (2007).

[22] V. V. Laguta and M. Nikl, Phys. Status Solidi B **250**, 254 (2013).

[23] A. I. Becerro and A. Escudero, Phase Transit. **77**, 1093 (2004).

[24] T. Gustafsson, M. Klintenberg, S. E. Derenzo, M. J. Weber, and J. O. Thomas, Acta Cryst. C **57**, 668 (2001).

[25] M. Nikl, V. V. Laguta, and A. Vedda, Phys. Status Solidi B **245**, 1701 (2008).

[26] C. Ezzeh and B. R. McGarvey, J. Chem. Phys. **61**, 2675 (1974); Z. Šroubek and K. Ždansky, *ibid.* **44**, 3078 (1966).

[27] O. F. Schirmer and K. A. Müller, Phys. Rev. B **7**, 2986 (1973).

[28] A. Abragam, J. Horowitz, and M. H. L. Price, Proc. Roy. Soc. (London) A **230**, 169 (1955).

[29] B. R. McGarvey, J. Phys. Chem. **71**, 51 (1967); M. Greenblatt and P. Strobel, J. Chem. Phys. **74**, 6580 (1981).

[30] R. D. Shannon, Acta Crystallogr. A **32**, 751 (1976).

[31] T. Kärner, V. V. Laguta, M. Nikl, and S. Zazubovich, Phys. Status Solidi B **251**, 741 (2014).

[32] O. F. Schirmer, J. Phys.: Condens. Matter **18**, R667 (2006).

[33] M. H. L. Pryce, Proc. Phys. Soc. Lond. A **63**, 25 (1950).

[34] H. R. Zeller and W. Känzig, Helv. Phys. Acta **40**, 845 (1967); W. Känzig and M. H. Cohen, Phys. Rev. Lett. **3**, 509 (1959).

[35] H. Seidel and H. C. Wolf, in *Physics of Color Centers*, edited by W. Beall Fowler (Academic Press, New York and London, 1968), pp. 538–619.

[36] D. S. Gough, P. Hannaford, and R. J. McLean, J. Phys. B: At. Mol. Opt. Phys. **21**, 547 (1988).

[37] M. Springis, A. Pujats, and J. Valbis, J. Phys.: Condens. Matter **3**, 5457 (1991).

[38] V. V. Laguta, M. Nikl, A. Vedda, E. Mihokova, J. Rosa, and K. Blazek, Phys. Rev. B **80**, 045114 (2009).

[39] R. Ramírez, M. Tardío, R. González, J. E. Muñoz Santiuste, and M. R. Kokta, J. Appl. Physics **101**, 123520 (2007).

[40] V. Jary, A. Krasnikov, M. Nikl, and S. Zazubovich, Phys. Status Solidi B (to be published).

[41] V. V. Laguta, M. Nikl, and S. Zazubovich, Opt. Mater. **36**, 1636 (2014).

[42] V. V. Laguta, A. M. Slipenyuk, J. Rosa, M. Nikl, A. Vedda, K. Nejezchleb, and K. Blazek, Radiation Measurements **38**, 735 (2004).

[43] Kh. S. Bagdasarov, Yu. N. Dubrov, I. N. Marov, V. O. Martirosyan, and M. L. Mailman, Phys. Status Solidi B **56**, K65 (1973).

[44] V. V. Laguta, A. M. Slipenyuk, M. D. Glinchuk, M. Nikl, J. Rosa, A. Vedda, and K. Nejezchleb, Opt. Mater. **30**, 79 (2007).

[45] P. Höfer, A. Grupp, H. Nebenführ, and M. Mehring, Chem. Phys. Lett. **132**, 279 (1986).

[46] A. Schweiger and G. Jeschke, *Principles of Pulse Electron Paramagnetic Resonance* (Oxford University Press, New York, 2001).